HHS Public Access

Author manuscript

*Comput Biol Med*. Author manuscript; available in PMC 2017 August 01.

Published in final edited form as:

*Comput Biol Med*. 2016 August 1; 75: 38–44. doi:10.1016/j.compbiomed.2016.05.008.

# Visualization of Electrical Field of Electrode Using Voltage-Controlled Fluorescence Release

**Wenyan Jia**[a], **Jiamin Wu**[b], **Di Gao**[b], **Hao Wang**[c], and **Mingui Sun**[a,c]

[a]Departments of Neurosurgery, University of Pittsburgh, PA, USA, 15260

[b]Departments of Chemical and Petroleum Engineering, University of Pittsburgh, PA, USA, 15260

[c]Departments of Electrical and Computer Engineering, University of Pittsburgh, PA, USA, 15260

## Abstract

In this study we propose an approach to directly visualize electrical current distribution at the electrode-electrolyte interface of a biopotential electrode. High-speed fluorescent microscopic images are acquired when an electric potential is applied across the interface to trigger the release of fluorescent material from the surface of the electrode. These images are analyzed computationally to obtain the distribution of the electric field from the fluorescent intensity of each pixel. Our approach allows direct observation of microscopic electrical current distribution around the electrode. Experiments are conducted to validate the feasibility of the fluorescent imaging method.

### Keywords

Electrical current distribution; Fluorescent tracer; Electrode-electrolyte interface

## 1. Introduction

Understanding the interface between biosensors and living systems has been one of the greatest challenges in the field of biomedical engineering. It requires a confluence of studies in not only engineering, life science, but chemistry, physics, mathematics, and other fields [1]. Biopotential electrodes, which are used to record electric activities of living cells or deliver electric currents, allow current flow across the interface between electronic measurement circuit and biological tissue [2]. To evaluate the performance of electrode, impedance of the electrode-electrolyte/tissue interface is always an important variable because it facilitates charge transfer between electrolyte and electrode. With a low impedance electrode, high-quality signal can be obtained during recording (e.g., electroencephalography) and the voltage applied to the tissue can be reduced during

**Correspondence to**: Department of Neurosurgery, University of Pittsburgh, Pittsburgh, PA 15260. Tel.: + 412 802 6475. wej6@pitt.edu.

stimulation (e.g., deep brain stimulation) [3]. Traditionally the impedance is measured using electrochemical impedance spectroscopy (EIS) [4], which is a popular method to study the electrode-electrolyte interface using a small-amplitude signal in varying frequencies. The interface is usually simplified as a combination of electronic circuit elements, and these elements are parameterized and identified through measurements by the EIS. Although different equivalent models (e.g., Warburg model and Randles model [2, 5]) have been proposed to study the electrochemical reaction occurred at the interface, the impedance has been considered a global property of the electrode, ignoring the structure of the electrode and the inhomogeneous nature of the electrolyte and the tissue.

Because current density distribution in local regions of an electrode is important in understanding electrode-tissue interaction, it is desirable to know how the current flows from the electrode to tissue and vice versa. Due to the inability of directly observing charge transfer at the interface, finite element model (FEM) has become a commonly used tool to visualize the electric field in the electrolyte [6–19]. If the FEM model is accurate in geometrical, electrical and material properties, the current/voltage can be calculated and visualized at each element (e.g., tetrahedra in 3D space). As a result, electrode geometry, material, and surface properties with respect to the surroundings of the electrode can be studied, and the results can be used to evaluate the performance of biopotential recording and the efficiency of electrical stimulation. McIntyre and his colleagues studied a conical metal microelectrode and found that the surface area, roughness, resistive coating of the electrode surface, and the radius of curvature of its tip affected the spatial distribution of the current over the surface of the electrode [8]. It has been shown that the activation of axons depends on the second-order spatial derivative of the extracellular potential [20, 21]. Based on this result, high-perimeter planar electrodes have been developed to improve the efficiency of neural response to deep brain stimulation (DBS) by increasing the spatial non-uniformity of the current density around the electrode [13–15]. Kuncel and Grill provided a way to choose stimulation parameters for DBS by investigating the effects of electrode contact location and geometry on the electric field using FEM [17]. Yousif *et al*. constructed a FEM model of the electrode-brain interface with graded complexity in structure. This model was used to study the mechanism of DBS during the acute and post-implantation stages [18, 19]. To model the electrical potentials recorded in microelectrode arrays, Ness *et al*. established a biophysical forward model based on the FEM to link the neural activity in the brain tissue slice and the potentials recorded by microelectrode arrays [16]. Howell et al, studied the influences of electrode geometry, and the electrode–tissue interface on models of electric fields produced by DBS [6]. However, the FEM-based analysis has two major limitations: (1) the knowledge of the geometry and electrical property (i.e., conductivity) of each element of FEM is required which are difficult to measure for a living system, and (2) validating the modelled voltage/current distribution is difficult.

In order to image the current density directly at the electrolyte-electrode interface, the electrical current density vectors in electrolyte is measured using the current density imaging (CDI) [22–26]. The CDI, a type of magnetic resonance imaging method, was used to observe the current density distributions on the DBS electrode surface as well as in the electrolyte within several millimeters beneath the electrode on a homogenous gel phantom [26, 27]. However, this method can only visualize the pathway of the controlled alternating

electric currents and the spatial resolution of this method is low, in the order of millimeters. As a result, the CDI has mainly been used to solve the inverse problems of the current field in conductivity imaging [26, 28]. As an imaging mode for the atom force microscope, electric force microscopy measures the electric field gradient distribution above a sample surface by applying a voltage between the conductive tip of an electrode and the sample [29–31]. However, the measurement has to be conducted in an ultra-high vacuum environment and no conductive material is permitted between the tip and the electric field. This approach is suitable for applications such as distinguishing conductive and insulating regions in the printed circuit board rather than detecting current flowing in conductive electrolyte. In 1999, Maus and co-workers utilized electrically generated chemiluminescence to image the nonuniform current density in the vicinity of an electrode [32]. When excited by an alternative current, the chemiluminescence arising from reaction of radical cations of 9,10-diphenylanthracene (DPA) and benzonitrile (solvent) radical anions in the electrolyte were captured by fluorescent microscopy as an indicator of the current density. Although the spatial resolution could be as high as one micrometer, the electrolyte concentration (containing DPA) and the excitation frequency had to be optimized to achieve a high luminescent intensity. An experimental approach has also been undertaken to characterize the spatial distribution around an active stimulating electrode [33]. Implanted microelectrodes were used to record the voltages generated by the active electrode in a monkey animal model. The measurement results are compared with the voltages calculated from a finite element model. Although this approach is feasible, it is invasive and expensive.

Till now, visualization of electric field at the electrode-electrolyte interface remains an unsolved problem although fluorescent tracers have been available for the study of the interaction between the electrode and tissue. Fluorescent staining of neural tissue was used to study the inflammatory response by imaging the electrode-tissue interface with implanted electrodes [34]. Fluorescein derivatives have also been used for imaging of pH gradients in biological system [35–37]. Voltage-sensitive dye was applied to visualize the voltage change across the membrane of cell attached on a silicon chip [38].

In this work, we proposed to image the current distribution at the interface using voltage-controlled fluorescence release, inspired by the mechanism of electrically-controlled drug release [39, 40]. Different from those previous studies, we coat the electrode with a solution containing fluorescent tracer using electrochemical deposition, and then release the tracer by applying an electric potential across the interface. A high-speed fluorescent microscopy is used to capture the distribution of the tracer at different time points. By analyzing these images, the electric current distribution at the interface is calculated. Our method is easy to perform and no specific instrumentation is required except a use of fluorescent microscopy.

The rest of the paper is organized as follows. Section 2 describes the fluorescent tracer, a method to release the tracer, and a derivation of the current distribution in the fluorescent images. Section 3 and 4 present experimental design and results, respectively. Conclusion and discussion are provided Section 5.

## 2. Materials And Methods

### 2.1 Fluorescent Tracer

In order to image the electrode-electrode interface, fluorescein sodium salt (Sigma-Aldrich Corporation, St. Louis, MO) was used as a fluorescent tracer. The molecular radius of this salt is small and each molecule has two negative charges. Fluorescein is among the most common fluorescent dyes for many applications. Fluorescein sodium (see Figure 1) is a disodium salt of fluorescein that possesses a high solubility in water, equal to 500 mg $mL^{-1}$. These properties makes fluorescein sodium a good fluorescent tracer to investigate the working of electrodes.

### 2.2 Electrically Controlled Release of Fluorescent Tracer

The Polypyrrole (PPy) film was deposited on the electrode by one-step electropolymerization [38]. Negatively charged fluorescein as a dopant was incorporated into the PPy thin film to maintain charge neutrality during electrochemical oxidation. The doped PPy film can be reversibly switched between an oxidized state and a reduced state accompanied by the movement of dopant ions in and out of the polymer film for charge compensation. Therefore, upon the application of a negative electrical potential, PPy was reduced, expelling fluorescein anions from the PPy film. After the fluorescein anions were released from the PPy film, electric-field-driven migration plays an important role in the movement of negatively charged fluorescein in the electrolyte toward the opposite charged electrode. This procedure is illustrated in Figure 2.

### 2.3 Electric Field Imaging

Because the process of the fluorescence release can be captured by high-speed fluorescent microscopy and the fluorescent intensity of each pixel in the mages can be assumed to be proportional to the concentration of the fluorescent tracer at the location, we propose a computational method to calculate the distribution of the electric field from the captured image.

Let $V$ represent a given volume in the electrolyte between the active electrode and the ground electrode in 3D space. Eq. (1) holds in regions where no fluorescent tracer is injected, i.e., the inflow flux of the tracer equals the outflow flux in volume V

$$\frac{\partial}{\partial t}\iiint_V C_d dV = -\oiint_S (\boldsymbol{J}_d - \mu \boldsymbol{E} C_d)\boldsymbol{n} dS \quad (1)$$

where the left side is a volume integral over volume $V$, and the right side is a surface integral over its boundary $S$, $C_d$ is the concentration of the tracer, $\boldsymbol{J}_d$ is the diffusion flux of the tracer, μ is the electric mobility of the tracer in the electrolyte, $\boldsymbol{E}$ is the electric field, and $\mu\boldsymbol{E}$ represents the drift velocity.

From Fick's first law and electrostatic theory, we have

$$\boldsymbol{J}_d = -D\nabla C_d \quad (2)$$

and

$$\boldsymbol{E} = -\nabla U \quad (3)$$

where $D$ is the diffusion coefficient and is the electrical potential. Substituting (2) and (3) to (1), we get

$$\frac{\partial}{\partial t}\iiint_V C_d dV = -\oiint_S (-D\nabla C_d + \mu\nabla U C_d)\boldsymbol{n} dS \quad (4)$$

After applying Gauss's theorem, (4) can be rewritten as

$$\frac{\partial}{\partial t}\iiint_V C_d dV = -\iiint_V [\nabla \cdot (-D\nabla C_d + \mu\nabla U C_d)] dV \quad (5)$$

Therefore,

$$\iiint_V \left[\frac{\partial C_d}{\partial t} - D\nabla^2 C_d + \mu\nabla C_d \nabla U + \mu C_d \nabla^2 U\right] dV = 0 \quad (6)$$

Because no net charge exists between the active electrode and the ground, $\nabla^2 U = 0$. Thus we can get

$$\frac{\partial C_d}{\partial t} - D\nabla^2 C_d + \mu\nabla C_d \nabla U = 0 \quad (7)$$

Assuming that the intensity of the fluorescence is proportional to the concentration of the dye, we can set $I_d = k \cdot C_d$, where $I_d$ is the intensity in the fluorescent image and $k$ is a constant. Then, (7) becomes

$$\frac{\partial I_d}{\partial t} - D\nabla^2 I_d + \mu\nabla I_d \nabla U = 0 \quad (8)$$

Therefore,

$$-\nabla U = \left(\frac{\partial I_d}{\partial t} - D\nabla^2 I_d\right) / (\mu\nabla I_d) \quad (9)$$

Because $\boldsymbol{E} = -\nabla U$, we have

$$\boldsymbol{E} = \left( \frac{\partial I_d}{\partial t} - D\nabla^2 I_d \right) / (\mu \nabla I_d) \quad (10)$$

Since both the diffusion coefficient $D$ and the electric mobility μ are constant and can be determined by the properties of the tracer and electrolyte, $\boldsymbol{E}$ can be calculated from the images.

## 3. Experimental Design and Results

### 3.1 Electrode Preparation

In this experiment, we used the screw EEG electrode developed by our team [41–43]. This electrode has a cylinder shape (diameter=10mm), with microteeth around its bottom rim. The shape of these teeth has been specially designed so that the electrode can hold its position (i.e., affix itself) on the surface of the skin after penetrating the top layer of the scalp, see Fig. 3. These teeth are extended horizontally to grab the skin when twisted, limiting skin penetration to avoid pain and discomfort. This electrode can be applied and removed very quickly since neither skin preparation nor gel/paste is required. A stainless steel is used as the material for the electrode body to achieve the required hardness and flexibility. For mass production of the electrode, a photolithographic technique is adopted to manufacture the microteeth. Impedance are further reduced by increasing electrode contacting area with tissue and coating with gold [43].

### 3.2 Fluorescent Coating

Each electrode strip was first degreased by sonication for 20 minutes in 2 M KOH containing 200 mg/L of sodium dodecyl sulfate. After rinsing thoroughly with distilled water, the electrode was cleaned by acetone/ethanol sonication/ultra-violet ozone. Then, 200 nm thick Au was deposited on electrode strips by sputtering. Pyrrole was distilled under vacuum prior to use. Fluorescein sodium salt was used as the fluorescent probe. PPy doped with fluorescein sodium was electrodeposited onto the electrode surface at a constant current density of 1 μA/cm$^2$ for 30 seconds using 0.2 M pyrrole and 0.01 M sodium fluorescein solution. The platinum wire mesh was used as the counter electrode and Ag/AgCl as the reference electrode. The electrode was rinsed thoroughly with de-ionized water and stored in 0.5X Phosphate Buffered Saline (PBS) at 4°C.

### 3.3 Experimental Procedure

A cell culture dish with a diameter of 60mm was chosen as the container. The electrode strip was fixed on the bottom of the dish using tape. A long self-adhesive copper strip was used as the ground electrode. The layout of the electrode strip and ground, as well as a microscopic image of an electrode tip, are shown in Fig. 4. 0.5X PBS buffer was slowly dropped into the container until the electrodes are fully immersed. A constant-voltage power supply of −1.0 V was applied across the electrode strip and the self-adhesive copper strip electrode at room temperature to trigger the release of the florescent film. The distance between the two

electrodes is approximately 0.5 cm (shown in Figure 4a). The voltage was pre-determined with experiments. The release of fluorescein was monitored using a Carl Zeiss Axio Imager A1 fluorescent microscopy. The exposure time was set to 20ms.

### 3.4 Acquired Images

Figure 5 shows twenty concessive fluorescent images before and after triggering the tracer release, respectively. The interval between two images is 51ms. The change of the electrical current distribution around the electrode strip can be observed clearly after tracer releases. It can also be observed that the right side of the electrode, which is closer to the ground electrode, is highlighted first.

### 3.5 Image Analysis Results

In our case, the thickness of the electrode is small. Therefore, the pattern of the electrode is essentially two-dimensional. As a result, we can ignore the diffusion of the tracer in the third dimension along the thickness, and the 2D imaging in Fig. 5 is sufficient to observe the electrical activity of the electrode. Since Eq.(1) can only be applied to the region between the active electrode and the ground electrode, we first extracted the boundary of the electrode from the image using Canny edge detection algorithm, shown in Fig. 6(a). The temporal changes of intensity at four boundary points of the electrode are illustrated in Fig. 6(b). It can be seen that the intensity values at some locations change faster than those at other locations, which demonstrates different speed of tracer release at different locations. Using the time for each pixel to reach the maximum intensity as an indicator of the release speed, a map of the speed of release is shown in Fig. 6(c) where the following nonlinear normalization was used to adjust the dynamic range of the image so that pixel intensity variations can be observed more clearly.

$$I_T = \sqrt[2]{I_O} \quad (11)$$

$$I_N = (I_T - \mathrm{Min}(I_T))/(\mathrm{Max}(I_T) - \mathrm{Min}(I_T)) \quad (12)$$

where $I_O$ and $I_N$ represent, respectively, the pixel values before and after normalization, $I_T$ is the intermediate value after the nonlinear transform.

We calculated the electric field distribution outside the electrode according to Eqs. (10). In this calculation, the diffusion coefficient $D$ was set to $2.7\times10^{-6}$ $cm^2/s$, and the electric mobility μ is computed to be $2.206 \times 10^{-8}$ $m^2/(Vs)$ using the Einstein–Smoluchowski relation. In our case, the spatial resolution of the image is approximately 2.5μ$m$, which corresponds to the distance between two adjacent pixels. Fig. 7 shows the amplitude of the electric field calculated from Figs. 5(b) and (c), and Figs 5(c) and (d). The computation results from subsequent frames show similar patterns. The same normalization as in Fig 6(c) is used in Fig.7. These results show that the current distribution is quite complex, depending

on the local geometric shape of the electrode. For clarity, pseudo color is used to plot Fig. 7(b) and (c). Because of the larger value of local curvature, the amplitude of the electric field around the tip is generally higher than other regions.

## 4. Conclusion

In this study, we demonstrated a proof-of-concept experimental approach to obtain an electric field map around electrodes in a heterogeneous environment. We presented an imaging method using fluorescent tracer and a computational method to calculate the electric field distribution from the acquired microscopic images when voltage-controlled fluorescent tracer was released. These methods can be used to directly visualize the electrical current or electric field distribution at the electrode-electrolyte interface, regardless of the shape of the electrode.

## 5. Discussions

The release process of fluorescein anions under an electric field is a complex process to model. The diffusion migration model used in our calculation is built outside the polypyrrole film (i.e. the model is built for the region between the surface of the polyprrole film and the counter-electrode surface, which is filled with solution). The electric field is calculated based on the fluorescent signal using a simple numerical method. Because the fluorescent signal is read directly by an experimental approach, the effect of the boundary conditions, including the dye release from the polypyrrole film, are already included in our calculation, and we believe the result is a good representation of electric field mapping inside the solution. We will improve the dye migration model in the future to get more insight and accuracy of the electric field.

The proposed dye migration model can be used for deriving 3-dimensional electric field maps. Because in our current experiment, the fluorescent signal is obtained by using a fluorescent scope that only yields 2D images, only 2D E-maps are derived, which are actually good representation of the electric field in the thin film used in our experiment. However, the electric density in the third dimension cannot be entirely neglected, as shown in Fig. 5. Should the experimental setup allow us to take 3D fluorescent signals, 3D mapping of the electric field would be possible by using the same model.

A high-speed and high-resolution microscope is required to obtain the movement of the fluorescent tracer. In our previous study [44], the images were acquired at every second, which could not be used to derive the electric current distribution using the proposed method. But the distribution of fluorescent intensity was consistent with this study.

In addition, the density of the coated tracer must be controlled carefully to avoid fluorescent saturation in acquired images because, if saturation occurs, the fluorescent intensity in the image will be no longer proportional to the concentration of the dye. Furthermore, the density of the tracer has to be uniformly distributed on the surface of the electrode. We are investigating a new strategy to coat a uniform layer of the tracer on the electrode during the electrodeposition process.

## Acknowledgments

This work was supported by National Institutes of Health grants R01EB013174, U54EB007954, and Point-of-Care Center for Emerging Neuro-Technologies (POC-CENT).

## References

1. Neuman MR. Grand Challenges in Biomedical Engineering. Ieee Pulse. 2013; 4:3–4.
2. Neuman, MR. Biopotential electrodes. In: Webster, JG., editor. Medical Instrumentation - Application and Design. 3rd. John Wiley & Sons, Inc; 1998.
3. Franks W, Schenker I, Schmutz P, Hierlemann A. Impedance characterization and modeling of electrodes for biomedical applications. IEEE Trans Biomed Eng. 2005; 52:1295–1302. [PubMed: 16041993]
4. Orazem, ME.; Tribollet, B. Electrochemical impedance spectroscopy. New Jersey: John Wiley & Sons; 2008.
5. Geddes LA. Historical evolution of circuit models for the electrode-electrolyte interface. Ann Biomed Eng. 1997; 25:1–14. [PubMed: 9124725]
6. Howell B, Naik S, Grill WM. Influences of interpolation error, electrode geometry, and the electrode-tissue interface on models of electric fields produced by deep brain stimulation. IEEE Trans Biomed Eng. 2014; 61:297–307. [PubMed: 24448594]
7. Butson CR, McIntyre CC. Role of electrode design on the volume of tissue activated during deep brain stimulation. Journal of Neural Engineering. 2006; 3:1–8. [PubMed: 16510937]
8. McIntyre CC, Grill WM. Finite element analysis of the current-density and electric field generated by metal microelectrodes. Ann Biomed Eng. 2001; 29:227–235. [PubMed: 11310784]
9. Wei XF, Grill WM. Current density distributions, field distributions and impedance analysis of segmented deep brain stimulation electrodes. J Neural Eng. 2005; 2:139–147. [PubMed: 16317238]
10. Butson CR, Maks CB, McIntyre CC. Sources and effects of electrode impedance during deep brain stimulation. Clin Neurophysiol. 2006; 117:447–454. [PubMed: 16376143]
11. McIntyre CC, Mori S, Sherman DL, Thakor NV, Vitek JL. Electric field and stimulating influence generated by deep brain stimulation of the subthalamic nucleus. Clin Neurophysiol. 2004; 115:589–595. [PubMed: 15036055]
12. Cardu R, Leong PH, Jin CT, McEwan A. Electrode contact impedance sensitivity to variations in geometry. Physiol Meas. 2012; 33:817–830. [PubMed: 22531168]
13. Wei XF, Grill WM. Analysis of high-perimeter planar electrodes for efficient neural stimulation. Front Neuroeng. 2009; 2:1–10. [PubMed: 19194527]
14. Howell B, Grill WM. Evaluation of high-perimeter electrode designs for deep brain stimulation. Journal of Neural Engineering. 2014; 11
15. Golestanirad L, Elahi B, Molina A, Mosig Juan R, Pollo C, Chen R, et al. Analysis of fractal electrodes for efficient neural stimulation. Frontiers in Neuroengineering. 2013; 8:1–10.
16. Ness TV, Chintaluri C, Potworowski J, Leski S, Glabska H, Wojcik DK, et al. Modelling and Analysis of Electrical Potentials Recorded in Microelectrode Arrays (MEAs). Neuroinformatics. 2015
17. Kuncel AM, Grill WM. Selection of stimulus parameters for deep brain stimulation. Clin Neurophysiol. 2004; 115:2431–2441. [PubMed: 15465430]
18. Yousif N, Bayford R, Wang S, Liu X. Quantifying the effects of the electrode-brain interface on the crossing electric currents in deep brain recording and stimulation. Neuroscience. 2008; 152:683–691. [PubMed: 18304747]
19. Yousif N, Liu X. Investigating the depth electrode-brain interface in deep brain stimulation using finite element models with graded complexity in structure and solution. J Neurosci Methods. 2009; 184:142–151. [PubMed: 19596028]
20. Rattay F. Analysis of models for extracellular fiber stimulation. IEEE Trans Biomed Eng. 1989; 36:676–682. [PubMed: 2744791]

21. Rattay F. Analysis of models for external stimulation of axons. IEEE Trans Biomed Eng. 1986; 33:974–977. [PubMed: 3770787]
22. Joy M, Scott G, Henkelman M. In vivo detection of applied electric currents by magnetic resonance imaging. Magn Reson Imaging. 1989; 7:89–94. [PubMed: 2918822]
23. Pesikan P, Joy MLG, Scott GC, Henkelman RM. Two-dimensional current-density imaging. Ieee T Instrum Meas. 1990; 39:1048–1053.
24. Scott GC, Joy MLG, Armstrong RL, Henkelman RM. Measurement of Nonuniform Current-Density by Magnetic-Resonance. Ieee T Med Imaging. 1991; 10:362–374.
25. Scott GC, Joy MLG, Armstrong RL, Henkelman RM. Sensitivity of Magnetic-Resonance Current-Density Imaging. Journal of Magnetic Resonance. 1992; 97:235–254.
26. Joy, ML. MR current density and conductivity imaging: the state of the art. Proc 26th Annual International Conference of the Engineering in Medicine and Biology Society; 2007/02/03; San Francisco, CA. 2004. p. 5315-5319.
27. Patriciu, A.; DeMonte, TP.; Joy, MLG.; Struijk, JJ. Investigation of current densities produced by surface electrodes using finite element modeling and current density imaging. 23rd Annual International Conference on Engineering in Medicine and Biololgy Society; Turkey. 2001. p. 1157
28. Joy ML, Lebedev VP, Gati JS. Imaging of current density and current pathways in rabbit brain during transcranial electrostimulation. IEEE Trans Biomed Eng. 1999; 46:1139–1149. [PubMed: 10493077]
29. Girard P. Electrostatic force microscopy: principles and some applications to semiconductors. Nanotechnology. 2001; 12:485–490.
30. Barisci JN, Stella R, Spinks GM, Wallace GG. Study of the surface potential and photovoltage of conducting polymers using electric force microscopy. Synthetic Met. 2001; 124:407–414.
31. Lekkala S, Marohn JA, Loring RF. Electric force microscopy of semiconductors: Theory of cantilever frequency fluctuations and noncontact friction. Journal of Chemical Physics. 2013; 139
32. Maus RG, McDonald EM, Wightman RM. Imaging of nonuniform current density at microelectrodes by electrogenerated chemiluminescence. Anal Chem. 1999; 71:4944–4950. [PubMed: 21662840]
33. Miocinovic S, Lempka SF, Russo GS, Maks CB, Butson CR, Sakaie KE, et al. Experimental and theoretical characterization of the voltage distribution generated by deep brain stimulation. Exp Neurol. 2009; 216:166–176. [PubMed: 19118551]
34. Holecko MM 2nd, Williams JC, Massia SP. Visualization of the intact interface between neural tissue and implanted microelectrode arrays. J Neural Eng. 2005; 2:97–102. [PubMed: 16317233]
35. Lin HJ, Herman P, Lakowicz JR. Fluorescence lifetime-resolved pH imaging of living cells. Cytometry Part A : the journal of the International Society for Analytical Cytology. 2003; 52:77–89. [PubMed: 12655651]
36. Hanson KM, Behne MJ, Barry NP, Mauro TM, Gratton E, Clegg RM. Two-photon fluorescence lifetime imaging of the skin stratum corneum pH gradient. Biophys J. 2002; 83:1682–1690. [PubMed: 12202391]
37. Liebsch G, Klimant I, Krause C, Wolfbeis OS. Fluorescent imaging of pH with optical sensors using time domain dual lifetime referencing. Anal Chem. 2001; 73:4354–4363. [PubMed: 11569831]
38. Braun D, Fromherz P. Imaging neuronal seal resistance on silicon chip using fluorescent voltage-sensitive dye. Biophys J. 2004; 87:1351–1359. [PubMed: 15298937]
39. Pernaut JM, Reynolds JR. Use of conducting electroactive polymers for drug delivery and sensing of bioactive molecules. A redox chemistry approach. Journal of Physical Chemistry B. 2000; 104:4080–4090.
40. George PM, LaVan DA, Burdick JA, Chen CY, Liang E, Langer R. Electrically controlled drug delivery from biotin-doped conductive polypyrrole. Adv Mater. 2006; 18:577–581.
41. Sun, M.; Sclabassi, RJ.; Liang, W.; Marcanio, J. Skin-screw electrodes, University of Pittsburgh, US 12/012,607. 2012.
42. Sun, M.; Jia, W.; Liang, W.; Sclabassi, RJ. A low-impedance, skin-grabbing, and gel-free EEG electrode. Proc 34th Annual International Conference of the Engineering in Medicine and Biology Society; 2013/02/01; San Diego, CA. 2012. p. 1992-1995.

43. Sun M, Sclabassi RJ, Liang W, Marcanio J. Skin-Screw Electrodes. 2012

44. Jia, W.; Wu, J.; Gao, D.; Sun, M. Microscopic imaging of electrical current distribution at the electrode-electrolyte interface. 36th Annual International Conference of the IEEE Engineering in Medicine and Biology Society; Chicago, IL. 2014. p. 4252-4255.

## Biographies

Wenyan Jia received the Ph.D. degree in biomedical engineering from Tsinghua University, Beijing, China, in 2005. She is currently a Research Assistant Professor in the Department of Neurosurgery, University of Pittsburgh, Pittsburgh, PA. Her research interests include wearable sensors and signal/image processing in the field of healthcare.

Jiamin Wu received the Ph.D. degree in Chemical Engineering from University of Pittsburgh in 2012. He is a post-doctoral research associate in the Department of Chemical & Petroleum Engineering at University of Pittsburgh, USA. His current research interests focus on development of new materials and fabrication technology for energy and biomedical applications.

Di Gao received the B.S. degree in both Chemical Engineering and Computer Science from Tsinghua University, Beijing, China, in 1999 and the PhD degree in Chemical Engineering, University of California, Berkeley, 2004. He is an Associate Professor in the Department of Chemical and Petroleum Engineering, University of Pittsburgh. His research interests include applied nanomaterials and surface science, solar cells, and biosensors.

Hao Wang received his B.S. degree in electrical engineering from Tsinghua University, Beijing, China, in 2009, and M.S. degrees in electrical engineering from University of Pittsburgh, in 2012. He is currently a Ph.D. candidate in the Department of Electrical Engineering, University of Pittsburgh. His research interests include wireless power transmission, signal processing and machine learning.

Mingui Sun received the B.S. degree from the Shenyang Chemical Engineering Institute, Shenyang, China, in 1982, and the M.S. and Ph.D. degrees in electrical engineering from the University of Pittsburgh, Pittsburgh, PA, in 1986 and 1989, respectively. In 1991, he joined the faculty at the University of Pittsburgh, where he is currently a Professor in neurosurgery, electrical and computer engineering, and bioengineering. He has authored or coauthored more than 400 papers. His current research interests include wearable biomedical electronic devices, biomedical signal and image processing, sensors and transducers, as well as biomedical instruments.

## Highlights

- Electrical current distribution of an irregularly shaped electrode at the electrode-electrolyte interface is a significant but unsolved problem.
- The current distribution at the interface is imaged by fluorescent microscopy when voltage-controlled fluorescent tracer is released from the surface of the electrode.
- A computational method to calculate the distribution of the electric field from acquired fluorescent images is derived.

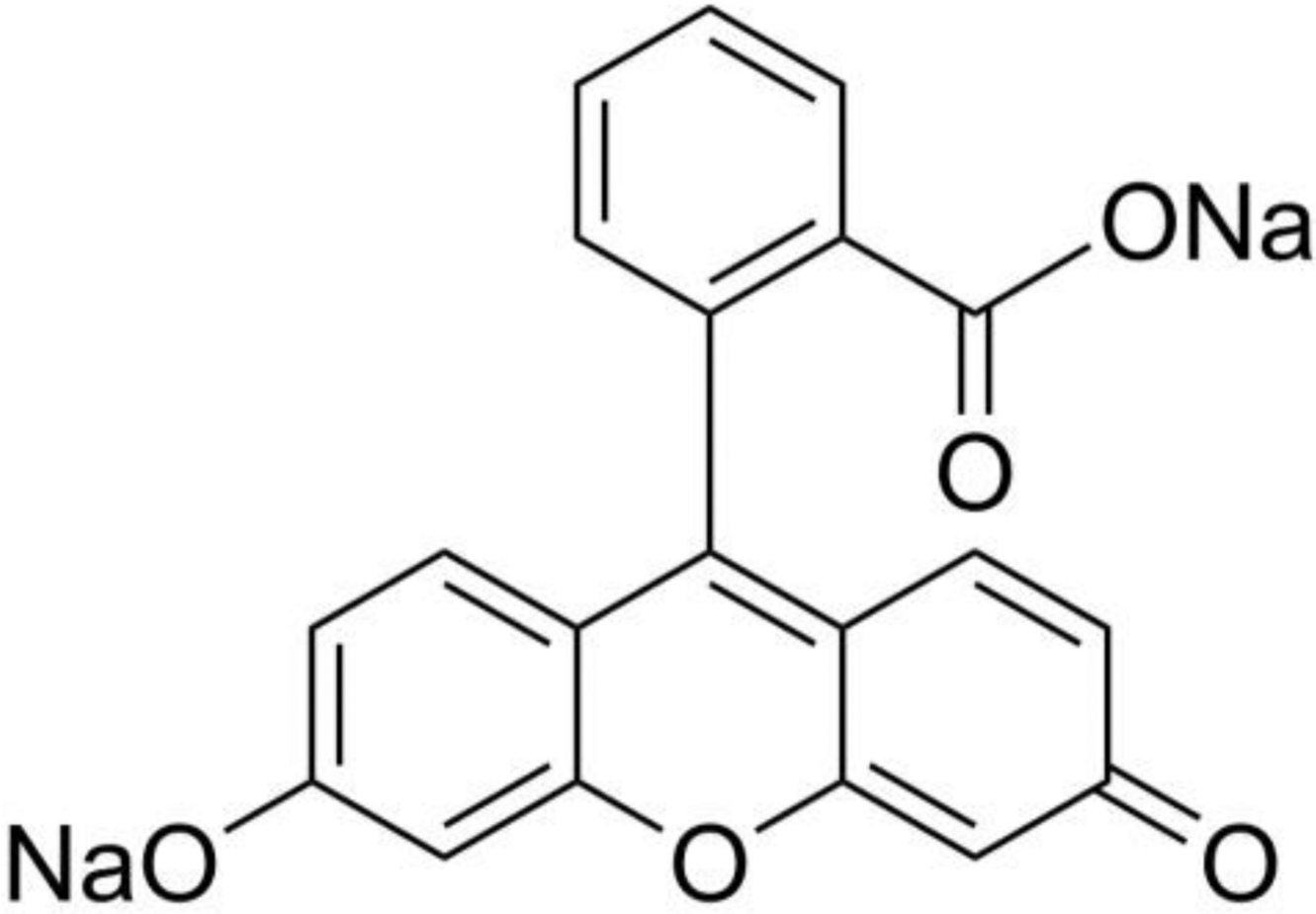


**Figure 1.**
Chemical structure of fluorescein sodium

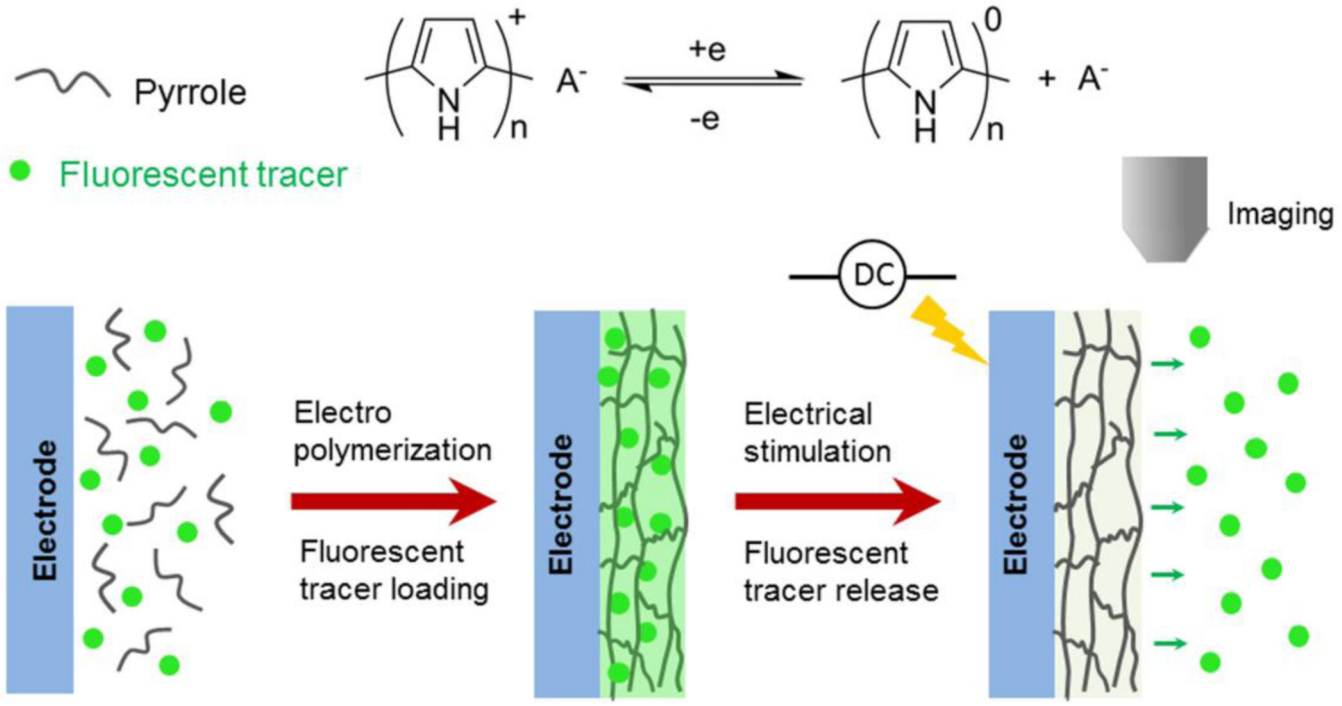


**Figure 2.**

Schematic illustration of electrically controlled release of fluorescent tracer for imaging and Redox reaction of PPY-A

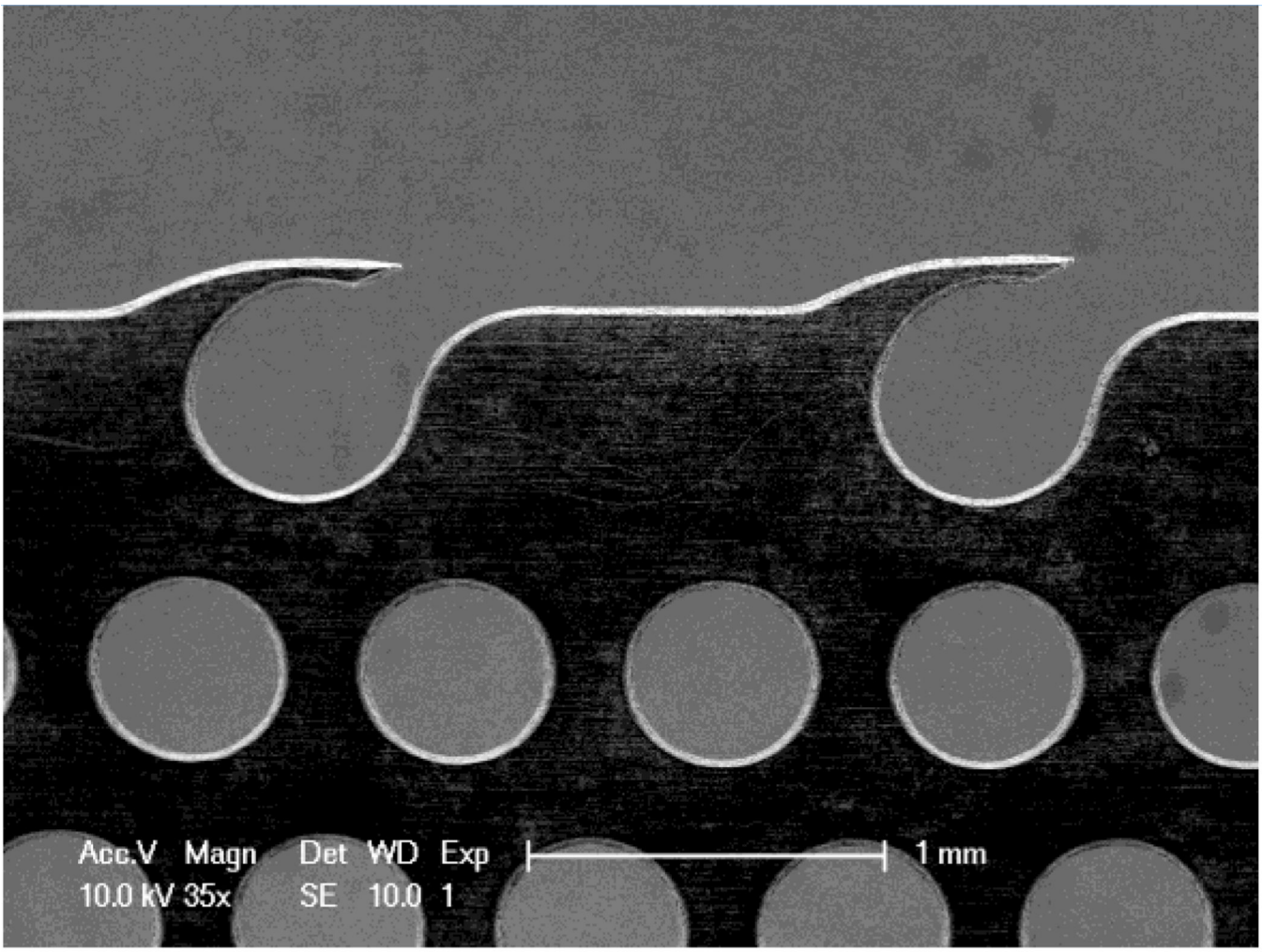


**Figure 3.**
Scanning electron microscope picture of the microteeth.

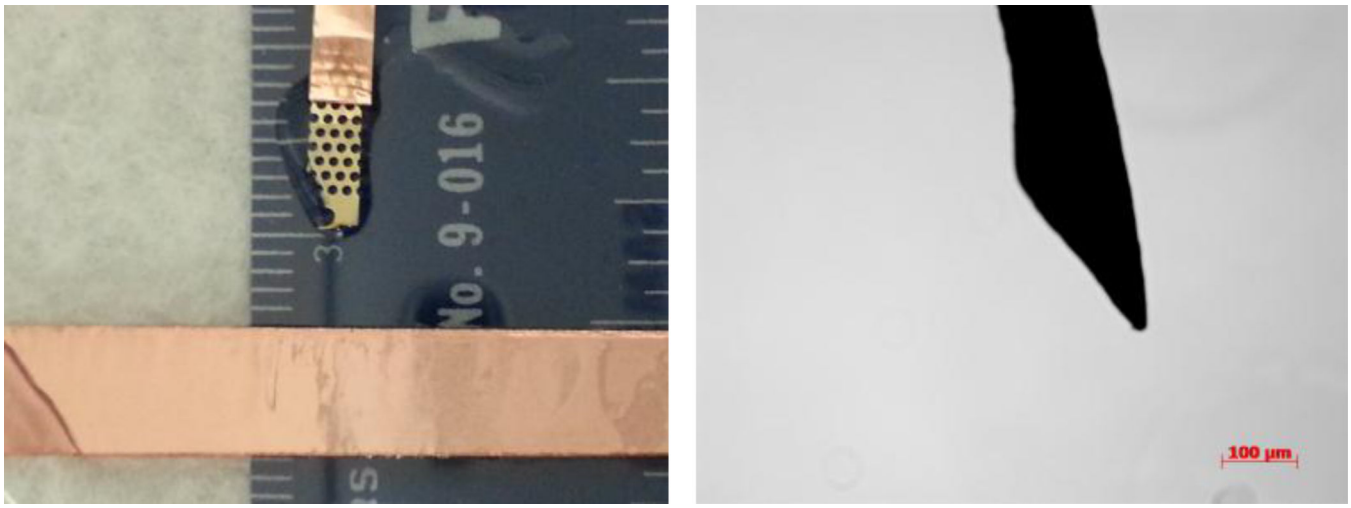


**Figure 4.**
Layout of the tested electrode and the ground (a) and the microscopic image of the electrode tip (b)

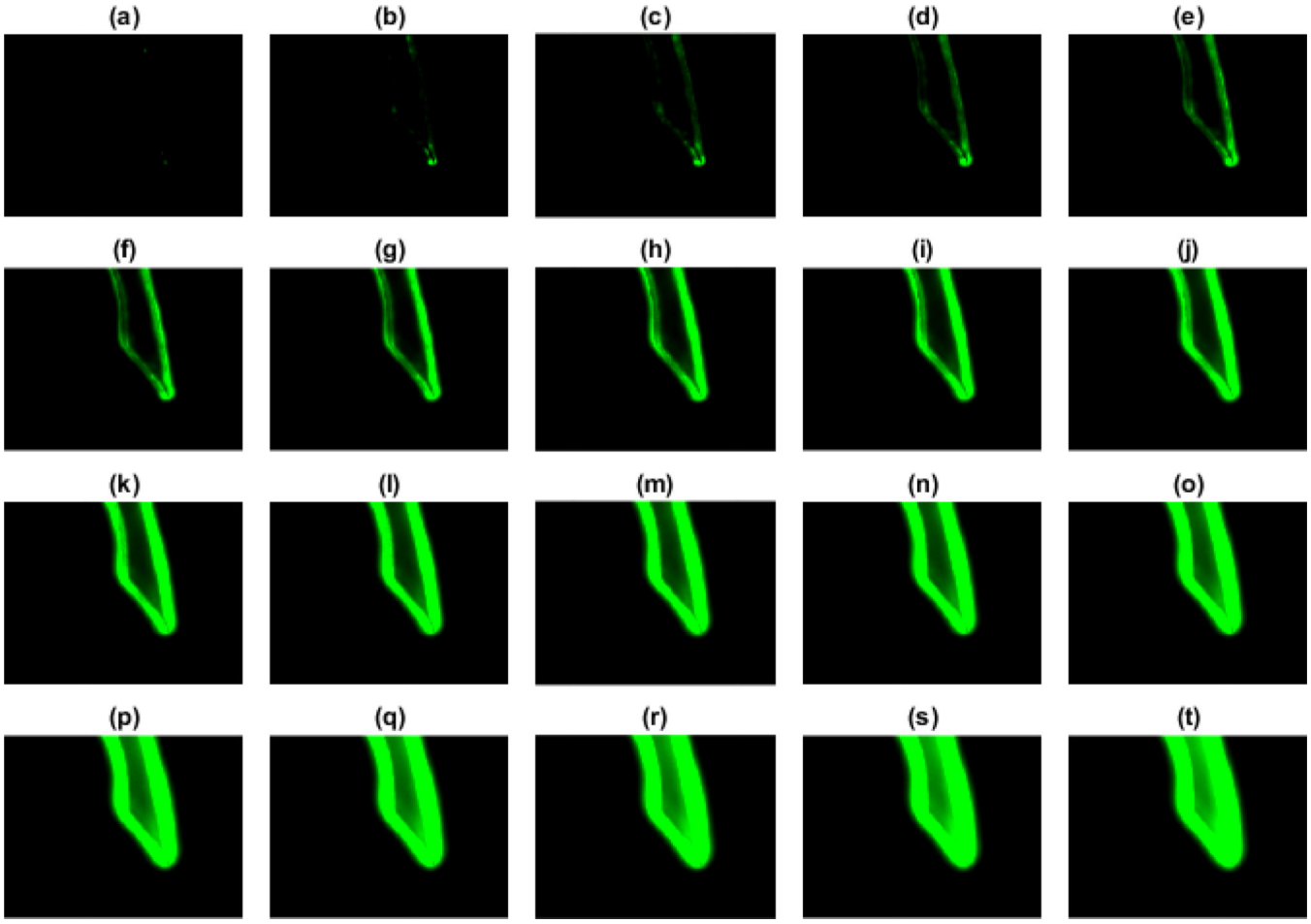


**Figure 5.**
(a)-(t) Twenty concessive fluorescent images acquired by the microscopy. (a) was obtained before the tracer was released.

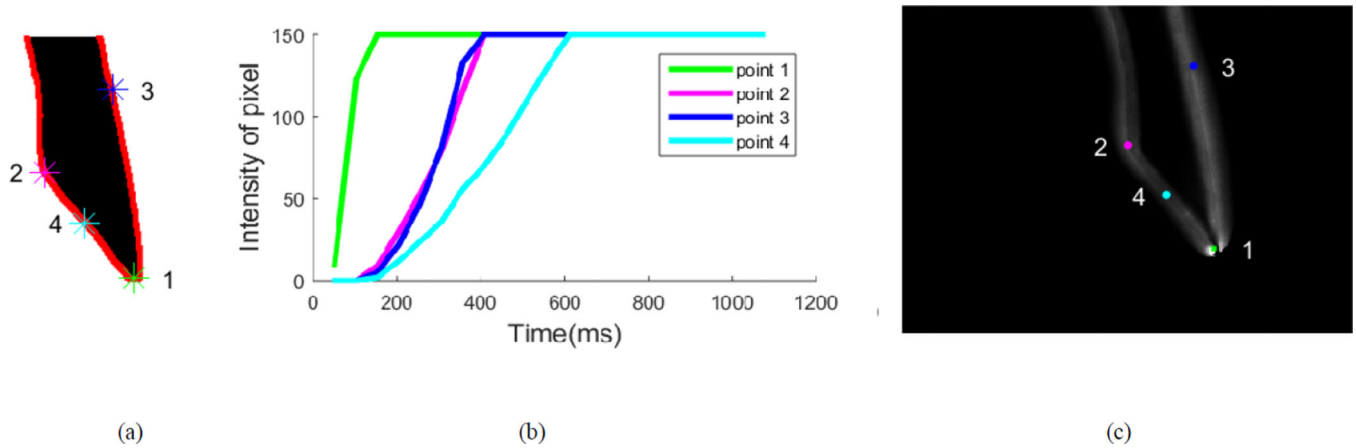


(a) (b) (c)

**Figure 6.**

(a) The electrode tip with extracted boundary with four marked boundary points; (b) the intensity changes with time at different locations, corresponding to the four points in (a); (c) A map of the release speed at each pixel, represented by the duration for that pixel to reach the maximum intensity. Nonlinear normalization was used when plotting the image to better display the change near the boundary.

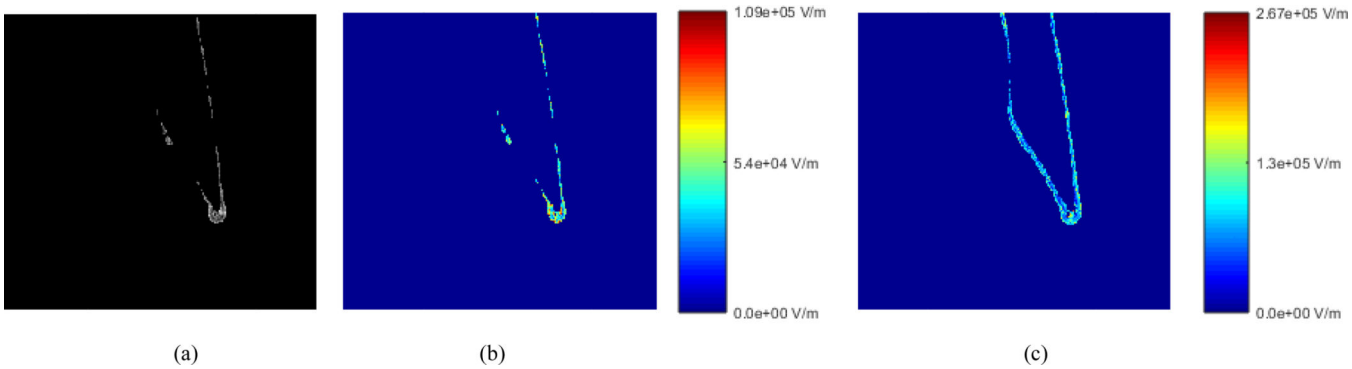


**Figure 7.**

(a) and (b) The amplitude of the calculated electric field from Figs 5(b) and (c); (c) The amplitude of the electric field from Figs 5(c) and (d).